

FASTIF: Scalable Influence Functions for Efficient Model Interpretation and Debugging

Han Guo^{1,2} Nazneen Fatema Rajani¹ Peter Hase²
 Mohit Bansal² Caiming Xiong¹

¹Salesforce Research ²UNC Chapel Hill
 {nazneen.rajani, cxiong}@salesforce.com
 {hanguo, peter, mbansal}@cs.unc.edu

Abstract

Influence functions approximate the “influences” of training data-points for test predictions and have a wide variety of applications. Despite the popularity, their computational cost does not scale well with model and training data size. We present FASTIF, a set of simple modifications to influence functions that significantly improves their run-time. We use k -Nearest Neighbors (k NN) to narrow the search space down to a subset of good candidate data points, identify the configurations that best balance the speed-quality trade-off in estimating the inverse Hessian-vector product, and introduce a fast parallel variant. Our proposed method achieves about 80x speedup while being highly correlated with the original influence values. With the availability of the fast influence functions, we demonstrate their usefulness in four applications. First, we examine whether influential data-points can “explain” test time behavior using the framework of simulatability. Second, we visualize the influence interactions between training and test data-points. Third, we show that we can correct model errors by additional fine-tuning on certain influential data-points, improving the accuracy of a trained MNLI model by 2.6% on the HANS challenge set using a small number of gradient updates. Finally, we experiment with a data-augmentation setup where we use influence functions to search for new data-points unseen during training to improve model performance. Overall, our fast influence functions can be efficiently applied to large models and datasets, and our experiments demonstrate the potential of influence functions in model interpretation and correcting model errors.¹

1 Introduction

Language understanding systems are becoming ever more powerful with the recent advances in

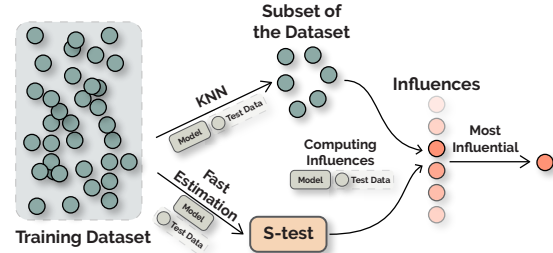


Figure 1: Workflow of our FASTIF w.r.t. a test data-point. First a subset of data-points are selected from the entire training set using k NN to reduce search space, then the inverse Hessian-vector product (s_{test}) is estimated based on Sec. 5.2. The influence values of data-points are computed using the outputs from these two steps. Finally, the most influential data-point(s) are returned.

large-scale pre-training. As these systems become widely adopted for real-world applications, the ability to interpret the model decisions grows increasingly important. An array of interpretation methods now exist for shedding light on models’ decision-making processes, with the bulk of work focusing on estimating feature importance (Li et al., 2016a; Ribeiro et al., 2016b; Lundberg and Lee, 2017; Sundararajan et al., 2017a; Ribeiro et al., 2018a) and interpreting internal model representations (Simonyan et al., 2014; Kim et al., 2018; Olah et al., 2018, 2020). These approaches aim to identify features a model uses to make decisions or analyze representations obtained from trained models. In contrast, one might also want to know how particular training data points influence model behavior at test time. This kind of goal is an instance of what Lipton (2016) terms “algorithmic transparency,” or, transparency “at the level of the learning algorithm itself.” The ability to do so would allow researchers to identify and respond to data responsible for problematic test-time behavior.

One simple brute-force way to estimate the importance of a training data-point to a test-time de-

¹Code is available at <https://github.com/salesforce/fast-influence-functions>.

cision is the leave-one-out approach (Hastie et al., 2009), i.e., train two models, one on the full training dataset, and the other on all but the training example to be considered. The difference in the behavior on the test data-point between these two models serves as a measure of the data influence. However, the computational cost of leave-one-out increases with model size and data size. To find the most influential data-point in the training set of size N , practitioners have to train $\mathcal{O}(N)$ models.

Alternatively, influence functions provide a tractable estimate of the effect without the need to repeatedly retrain the model. In a nutshell, the influence function estimates the impact on the model parameters when the loss of the training example is up-weighted by a small delta. Developed decades ago as a classic technique from robust statistics (Cook, 1977, 1986; Cook and Weisberg, 1980, 1982), influence functions have recently appeared in modern-scale machine learning (Koh and Liang, 2017) and have seen a wide of applications ranging from model interpretation to data valuation (Schulam and Saria, 2019; Brunet et al., 2019; Koh et al., 2018; Basu et al., 2020b; Koh et al., 2019; Feldman and Zhang, 2020; Koh et al., 2018; Schulam and Saria, 2019; Brunet et al., 2019; Koh et al., 2019; Basu et al., 2020b; Feldman and Zhang, 2020; Yang et al., 2020; Han et al., 2020; Ghorbani and Zou, 2019; Ghorbani et al., 2020; Jia et al., 2019b,a; Kwon et al., 2020).

Yet, influence functions are very expensive to compute for moderate-sized model and training data. For instance, finding the most influential examples w.r.t. an evaluation data-point with a model of about 14.7M parameters in a dataset of about 390K examples – a pretty moderate setting – takes more than 2 hours (see Sec. 3.5 for details). Consequently, applications might face the dilemma of either accepting the computation cost or resorting to a smaller-scale setting.² But why are influence functions computationally expensive? In our early experiments, we found that the main computational bottleneck lies in the following steps:

1. First, searching for the most positive/negative influential data-point(s) w.r.t. some evaluation data-point(s) is an $\mathcal{O}(n)$ operation (via enumerating the entire training set), and can take more than two hours in our experiments.

2. Second, estimating the inverse Hessian of model parameters required to compute the influence of a single data-point is expensive (usually in the order of minutes).
3. Lastly, previous algorithms perform serial computations that can actually be parallelized.

In this work, we present FASTIF (Fast Influence Functions) to address these challenges through three simple techniques. First, instead of enumerating the full training dataset to find influential data-point, we leverage fast nearest neighbor search (Johnson et al., 2017) to narrow the search to a small subset of influence-worthy data-points. This operation reduces the computation by about an order of magnitude. Second, we identify a set of hyperparameters for the Hessian estimation algorithm that reduces computation time by more than half while preserving estimation quality. Finally, we describe a simple parallelizable extension of the algorithm to leverage multiple GPUs, which gives an additional 2X speedup. As a result, we are able to improve the most influential examples search overall by approximately two orders of magnitudes in our experiments.

So what could we do with faster influence functions? We demonstrate the advantage of fast influence functions via several interesting downstream applications. These require computing influence functions repeatedly and were thus almost intractable without such fast influence functions:

1. First, while influential data-points contribute, by definition, significantly to the performance of the model on particular test data-point(s), it is not yet exactly clear how influential points “explain” model behavior. In Sec. 6.1 we examine the “explainability” of influential examples using the framework of simulatability Doshi-Velez and Kim (2017); Hase and Bansal (2020), and we find that they improve model simulatability.
2. Second, we visualize how different training data-points interact with different test data-points in Sec. 6.2. The visualizations help us uncover interesting latent structures in the dataset, and the insights could be used to improve model performance.
3. Third, in Sec. 6.3 we show a simple application of influence functions in correcting model prediction by fine-tuning on the right influential examples. Despite its simplicity, our method could improve a MultiNLI model’s accuracy on

²For instance, in Footnote 3 of Han et al. (2020) the authors mentioned that they had to resort to using a smaller model and dataset due to the computation cost.

the HANS dataset by more than 5% (about 2.6% more than our baseline).

4. Fourth, note that influence functions are defined w.r.t. the training data used in the model training. In Sec. 6.3, we extend the above experiment and demonstrate the potential of influence functions to the setting where we want to leverage a new dataset unseen during training.

2 Related Works

Explainable Machine Learning. With the rise of model complexity and adoption of large-scale machine learning models, there is an increasing emphasis on interpreting model behaviors (Doshi-Velez and Kim, 2017; Ribeiro et al., 2020; Wallace et al., 2019; Hase and Bansal, 2020). For example, previous works have considered interpreting predictions by constructing importance scores over the input tokens (Belinkov and Glass, 2019), attention-based methods (Jain and Wallace, 2019; Wiegrefe and Pinter, 2019; Zhong et al., 2019), gradient-based methods (Simonyan et al., 2013; Shrikumar et al., 2017; Sundararajan et al., 2017b; Smilkov et al., 2017; Feng et al., 2018), perturbation-based methods (Li et al., 2016b), local approximation methods (Ribeiro et al., 2016a, 2018b), prototype methods (Chen et al., 2019; Hase et al., 2019), counterfactual and decision boundary methods (Joshi et al., 2018; Samangouei et al., 2018; Mothilal et al., 2020), natural language generation (Camburu et al., 2018; Rajani et al., 2019; Hase et al., 2020; Wiegrefe et al., 2020), and recently, k NN-based methods (Papernot and McDaniel, 2018; Rajani et al., 2020).

Influence Functions. The use of influence-based diagnostics can be traced back to the '70s and '80s driven by seminal papers such as Cook (1977); Cook and Weisberg (1980, 1982); Cook (1986). Early work on influence functions focused on linear models and relatively small datasets, and later work extended this to more general models and a wider variety of perturbations (Chatterjee et al., 1986; Cook, 1986; Thomas and Cook, 1990; Wei et al., 1998; Faraway, 2016). Some of the early applications of influence functions in machine learning are on studying model robustness and fast cross-validation in kernel methods (Christmann and Steinwart, 2004; Debruyne et al., 2008; Liu et al., 2014).

Recently, Koh and Liang (2017) brought influ-

ence functions to large-scale deep learning and have been followed up by numerous subsequent works. For example, Koh et al. (2018) used them for data poisoning attacks, Schulam and Saria (2019) for calibrating trust in individual model predictions, Brunet et al. (2019) for tracing biases in word embeddings, Koh et al. (2019) and Basu et al. (2020b) for identifying important groups of training data, and Feldman and Zhang (2020) for studying neural network memorization. Finally, while the influence function we focus on in this work is related to the notion of leave-one-out, a generalized variant that measures leave- K -out (and marginalizes over K) has led to the concept of Data Shapley (Ghorbani and Zou, 2019; Ghorbani et al., 2020; Jia et al., 2019a,b; Kwon et al., 2020), which is rooted in game theory.

In the context of influence functions for NLP, Han et al. (2020) used them to explain model predictions and unveil data artifacts. Yang et al. (2020) used them to estimate the quality of synthetic training samples in the context of data-augmentation. Meng et al. (2020) explored the combination of gradient-based methods and influence functions to jointly examine training history and test stimuli. Their work also tried using influence functions to fix erroneously classified examples, albeit through retraining another model. In our work, we primarily focus on improving the run-time of the influence function, and explore their potential in interpreting model behaviors and efficiently correcting predictions. Kobayashi et al. (2020) experimented with the use of instance-specific dropout masks. Their method enables fast inference-time influence calculation but requires training the model with this specific type of dropout (called turn-over dropout). Our method, however, is an inference-time technique; it requires no change to model training and could, in principle, work with any trained model. Further, we include an extensive set of experiments/applications on a larger dataset.

3 FASTIF: Method Details

3.1 Background

Let a data-point be defined as $z = (x, y)$ for input $x \in \mathcal{X}$ and label $y \in \mathcal{Y}$, and the loss function be $L(z, \theta)$ that takes as input a data-point and a model parameterized by θ . Given N training data-points in the training set \mathcal{Z} , the standard empirical risk

	Original s_{test} (1 GPU)	Fast s_{test} (1 GPU)	Fast s_{test} (4 GPUs)
No $k\text{NN}$	≥ 2 hours (1X)	/	/
$k\text{NN } k = 1e4$	14.72 ± 0.21 min (8X)	6.61 ± 0.03 min (18X)	2.36 ± 0.02 min (50X)
$k\text{NN } k = 1e3$	10.93 ± 0.04 min (10X)	3.13 ± 0.05 min (38X)	1.46 ± 0.07 min (82X)

Table 1: Speed of influence functions. All experiments are measured on MultiNLI dataset. The run-times are averages and standard deviations over 10 examples.

minimization tries to solve the following problem,

$$\hat{\theta} = \arg \min_{\theta} \frac{1}{N} \sum_{i=1}^N L(z_i, \theta) \quad (1)$$

We want to answer the question: what is the influence of a training data-point z on the learned model parameters θ and its behavior on a new test data-point z_{test} .

Leave-one-out methods take the “discrete” way: train two models, one on the full training dataset \mathcal{Z} , and one on the same dataset but with z removed. The difference in the behavior between these two models is the effect of z ’s presence (or absence). Among the many definitions of model behavior, in this work we mainly focus on the loss at the test data-point. Influence functions, on the other hand, answer this question via approximating it locally and measures the change in the model behavior via up-weighting the loss of the training data-point by ϵ . Thus the influence function refers to *the change in the model’s loss on the test data-point z_{test} if we up-weight the loss of training data-point z by ϵ ,*

$$\mathcal{I}(z, z_{\text{test}}) := \frac{dL(z_{\text{test}}, \hat{\theta}_{\epsilon, z})}{d\epsilon} \quad (2)$$

where $\hat{\theta}_{\epsilon, z}$ are the parameters of the model trained with training data-point z up-weighted by ϵ ,

$$\hat{\theta}_{\epsilon, z} = \arg \min_{\theta} \frac{1}{N} \sum_{i=1}^N \left(L(z_i, \theta) + \epsilon L(z, \theta) \right) \quad (3)$$

Measuring $\mathcal{I}(z, z_{\text{test}})$ via training another model is prohibitively expensive. The influence function (Koh and Liang, 2017) is a tractable approximation, which computes the following quantity:

$$\mathcal{I}(z, z_{\text{test}}) \approx -\nabla_{\theta} L(z_{\text{test}}, \hat{\theta})^T H_{\hat{\theta}}^{-1} \nabla_{\theta} L(z, \hat{\theta}) \quad (4)$$

where $\hat{\theta}$ is the original parameters of model trained using training data-points, and $H_{\hat{\theta}}$ is the Hessian of model parameters. For each test data-point z_{test} ,

we are usually interested in finding the most positively influential training data-points, and the most negatively influential training data-points.³ We can find the most positively influential (i.e., harmful) training data-points z^* by computing the influence values between z_{test} and each z in the training set,

$$z^* = \arg \max_{z \in \mathcal{Z}} \mathcal{I}(z, z_{\text{test}}) \quad (5)$$

where $\arg \max$ changes to $\arg \min$ for finding the most negatively influential (i.e., helpful) data-point. While a much more tractable approximation, this is still unscalable in practice for a few reasons.

First, enumerating all the data-points in the training set to find the $\arg \max/\arg \min$ influence values is expensive for large datasets. Second, evaluating the inverse-Hessian $H_{\hat{\theta}}^{-1}$ is very expensive for large neural-network models (Koh and Liang, 2017; Agarwal et al., 2017). In this work, we address those challenges by presenting simple but effective methods. We summarize the speed improvements in MultiNLI settings in Table 1 and Sec. 3.5, and our method in Fig. 1.

3.2 Speeding up the $\arg \max$ using $k\text{NN}$

A naive implementation of Eq. 5 is expensive because the computation cost grows with the dataset size. In practice, however, we are primarily concerned with data-points that are most influential. We hypothesize that we could constrain the expensive search to a subset of promising data points, $\hat{\mathcal{Z}} \subseteq \mathcal{Z}$, that are likely to be influential without significant impact on quality,

$$z^* = \arg \max_{z \in \hat{\mathcal{Z}}} \mathcal{I}(z, z_{\text{test}}) \quad (6)$$

Notice that the $\arg \max$ is now performed over $\hat{\mathcal{Z}} \subseteq \mathcal{Z}$. We select the subset $\hat{\mathcal{Z}}$ as the top- k nearest neighbors of z_{test} based on the ℓ_2 distance

³A training data-point is positively influential w.r.t. a test data-point if up-weighting its loss leads to higher loss on the test data-point. A negatively influential data-point is defined similarly. Another interpretation is that a positively influential training data-point is “harmful” w.r.t. the test data-point, and a negatively influential data-point is “helpful.”

between extracted features of the data-points following [Khandelwal et al. \(2019\)](#) and [Rajani et al. \(2020\)](#). This operation is extremely fast using highly-optimized nearest neighbor search libraries such as FAISS ([Johnson et al., 2017](#)). In Sec. 5.1, we will examine the quality of nearest neighbors in terms of retrieving influence-worthy data-points.

3.3 Speeding up the Inverse Hessian

The next computational bottleneck lies in estimating the inverse Hessian of model parameters in Eq. 4. Computing the Hessian for the full training dataset is expensive, and inverting it is similarly prohibitive: with n training data-points and p parameters, this computation requires $\mathcal{O}(np^2 + p^3)$ operations, and is very expensive for large dataset/model (please see Sec. 3 in [Koh and Liang \(2017\)](#) for details). We start by describing the method proposed in [Koh and Liang \(2017\)](#).

First, notice that for each test data-point z_{test} , we can pre-compute and cache the following quantity,

$$s_{\text{test}} = H_{\hat{\theta}}^{-1} \nabla_{\theta} L(z_{\text{test}}, \hat{\theta}) \quad (7)$$

We can then efficiently compute the influence for each training data-point z ,

$$\mathcal{I}(z, z_{\text{test}}) = -s_{\text{test}} \cdot \nabla_{\theta} L(z, \hat{\theta}) \quad (8)$$

Next, the method approximates s_{test} via a combination of (1) implicit Hessian-vector products (HVPs) to avoid explicitly computing/storing $H_{\hat{\theta}}^{-1}$, (2) using a mini-batch of data-points to obtain a stochastic unbiased estimate of the Hessian, and (3) Neumann Series (Sec 3.1 in [Agarwal et al. \(2017\)](#)) to iteratively estimate the inverse. We refer interested readers to [Agarwal et al. \(2017\)](#) for details regarding the LiSSA (Linear time Stochastic Second-Order Algorithm) algorithm and to Sec. 4.2 in [Koh and Liang \(2017\)](#) for details regarding non-convexity and non-convergence. The algorithm can be summarized as:

Step 1. Let $v := \nabla_{\theta} L(z_{\text{test}}, \hat{\theta})$, and initialize the inverse HVP estimation $\hat{H}_{0, \hat{\theta}}^{-1} v = v$.

Step 2. For $j \in \{1, 2, \dots, J\}$, recursively compute the inverse HVP estimation using a batch size B of randomly sampled data-point(s) z ,

$$\hat{H}_{j, \hat{\theta}}^{-1} v = v + \left(I - \hat{\nabla}_{\theta}^2 L(z, \hat{\theta}) \right) \hat{H}_{j-1, \hat{\theta}}^{-1} v \quad (9)$$

where J is a sufficiently large integer so that the above quantity converges.

Step 3. Repeat Step 1 and 2 for T times independently, and return the averaged inverse HVP estimations.

We can see that the computation cost and approximation quality depends on a few variables: J the number of recursive iterations, T the number of independent runs, and B the batch size. Typically J is chosen such that the approximation converges, the number of repetition is simply set $T=1$, and the batch size is set to the largest value that the GPU can afford. In our experiments in Sec. 5.2, we have the following observations. First, the computation cost and the quality of estimation is sensitive to B . Second, when B is small, increasing T could effectively improve the quality. These observations motivated us to propose a few simple changes:

- Choose a J so that approximation converges.
- Choose a small batch size. In our experiments, we found that even $B = 1$ suffices.
- Make up for the noisiness of small batch size using larger T , which can be distributed over multiple GPUs.

In Sec. 5.2, we conduct experiments to understand the speed-quality trade-off under various configurations.

3.4 Details on Parallelization

It is easy to see that many components in computing influence functions are inherently parallelizable. While one could apply off-the-shelf multi-GPU parallelization tools such as `nn.DataParallel` in PyTorch ([Paszke et al., 2019](#)), the cost of communicating large vectors between GPUs outweighs the benefits of parallelism.⁴

The modifications described in Sec. 3.2 and 3.3 are designed with this taken into account. In particular, the advantage of using multiple repetitions in Sec. 3.3 is that it allows parallel-computation effortlessly. We can apply asynchronous parallel computation to compute the s_{test} , use one synchronization point to average the result using `all-reduce`, and then asynchronously compute the influence of a subset of data-points that are pre-selected using k NN. Figure 2 illustrates the process.

⁴In our early experiments, we noticed that a naive application of data-parallelism provided minimal speedup, and might sometimes slow things down.

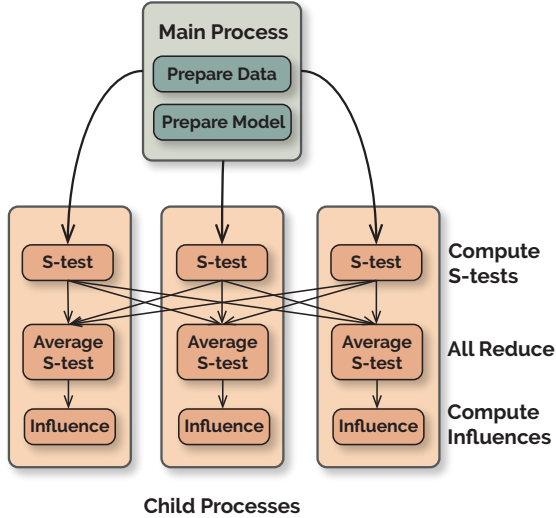


Figure 2: Parallel computation of influence functions. The main process prepares the data/model and sends these to child processes. Child processes (here with 3 GPUs) first compute local estimations of s -test. These are then aggregated using all-reduce. After the synchronization point, child processes have the same copy of the averaged s -test, and then they proceed to compute the influences of a subset of the data-points pre-selected via k NN.

3.5 Summary of Computation Times

Table 1 presents the summary of computation times. The run-time statistics (averages and standard deviations) are computed over 10 evaluation examples on the full MultiNLI training dataset (Williams et al., 2018) (please see Sec. 4 for details). We can see that adding k NN helps reduce the time by about an order of magnitude, fast s_{test} cuts the time by additional 55–70%, and parallelism further reduces the time by more than two fold. With $k = 1e3$, fast s_{test} approximation, and 4 GPUs, we are able to find influential training data-points of an evaluation data-point in about 1.5 minutes, more than 80 times faster than the original influence functions, which would take more than 2 hours.

4 Experimental Setup

We use the MultiNLI dataset in analysis experiments (Sec. 5) and both MultiNLI and HANS datasets (English) in the main experiments (Sec. 6) (McCoy et al., 2019; Williams et al., 2018).⁵ Our model is based on pre-trained BERT-base model fine-tuned on downstream tasks (Devlin

⁵When the model is intended to be used in both MultiNLI and HANS experiments, it is trained on the 2-label variant of MultiNLI. Please see Sec. 4 and Appendix D in McCoy et al. (2019) for details.

et al., 2019; Wolf et al., 2019). We freeze the first 9 layers based on results in Lee et al. (2019) to reduce computation cost, which leaves us with about 14.7M trainable parameters. We use weight decay of 0.005 during training following the evidence found in Basu et al. (2020a). Due to space consideration, for most of the experiments we include the motivation and results in the main paper. Please see the appendix for experiment details. Table 2 summarizes key experiment details such as the number of evaluation data-points and repetitions used in each of the experiments.

5 Analysis

In this section, we examine the effectiveness of the methods described in Sec. 3.2 and 3.3. Specifically, we conduct the following set of experiments:

- We measure k NN’s recall in terms of retrieving data-points that are potentially influential.
- We look at the trade-off in speed/quality of inverse Hessian-vector-product approximation with various configurations.
- We examine the quality of the influence estimations using all of the proposed techniques, by comparing the correlations between the influence values computed with/without them.

5.1 Recall of k NN

In Sec. 3.2, we describe the use of k NN for pre-selecting a subset of data-points. This (smaller) set of data-points are then re-ranked using the more expensive influence functions. Making this work well, however, requires that the subset of data-points selected by k NN contains potentially the most influential data-points.

In this section, we examine the k NN’s recall. We ask the question: *if a data-point is influential, will it be included in the subset selected by the k NN?* To formalize this, we define the recall score $R@m$ as the percentage of top- m ground-truth influential data-points that are selected by the k NN,

$$R@m = \frac{|\{ \text{retrieved} \} \cap \{ \text{top-}m \text{ influential} \}|}{|\{ \text{top-}m \text{ influential} \}|}$$

where we let the top- m influential data-points computed without k NN (i.e., on the full dataset) be the top- m ground-truth influential data-points.

Section	Details
Sec. 5.1	100 evaluation data-points, k NN with $k \in \{1 \times 10^1, 1 \times 10^2, 1 \times 10^3, 1 \times 10^4, 5 \times 10^4, 1 \times 10^5\}$, recall $R@m$ with $m \in \{10^1, 10^2, 10^3\}$.
Sec. 5.2	8 evaluation data-points, $J \in \{700, 800, \dots, 1300\}$, $B \in \{2^0, 2^1, \dots, 2^7\}$, $T \in \{1, 2, 3, 4\}$.
Sec. 5.3	6 evaluation data-points, k NN with $k \in \{10^3, 10^4\}$, $m_{\text{remove}} \in \{5^0, 5^1, 5^2\}$.
Sec. 6.1	20 evaluation data-points, 1 fine-tuning data-point, 50 learning rates in log-space from 10^{-5} to $10^{-2.5}$, and repeat for 10 different fine-tuning data-points.
Sec. 6.2	400 evaluation data-points where the model predictions are incorrect, including 100 from the MNLI evaluation dataset and 100 for each of the three subsets from the HANS evaluation dataset. We use k NN with $k = 10^3$.
Sec. 6.3	Experiments are repeated 3 times, 10 evaluation data-points used as the “anchor” data-points, fine-tuning is applied repeatedly for 10 iterations, and for each iteration, update parameters for one gradient step on 10 training data-points with learning rate 10^{-4} .

Table 2: Some of the key experiment details. Please see the appendix for full experiment details.

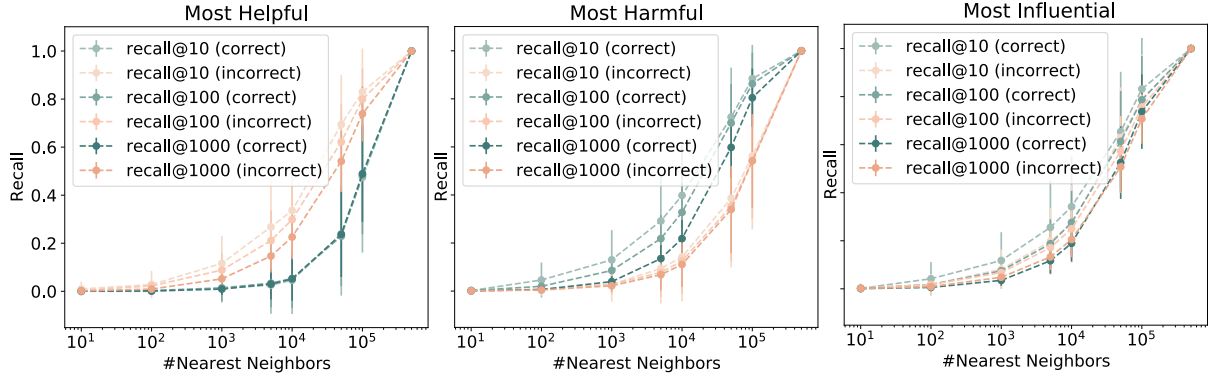


Figure 3: The recall of k NN in terms of finding influential data-points. The lines and error bars represent the means and standard deviations across 100 correct/incorrect predictions.

Results. Figure 3 shows the results of these experiments. Overall, the recall scores show that k NN is useful in selecting data-points that are likely to be influential. The recall scores for the most influential (i.e., using the absolute value) data-points are close to 60% with $k=5 \times 10^4$, and 20% with $k=5 \times 10^3$. These k ’s are about order(s) of magnitude smaller than the size of the full training dataset (more than 3.9×10^5 examples). Note that random selection would lead to recall around 15% ($k=5 \times 10^4$) and 1.5% ($k=5 \times 10^3$) in the two settings. One interesting observation is that, the recall scores for the most harmful data-points tend to be higher than the most helpful ones when the predictions are correct, but lower when the predictions are incorrect.⁶

5.2 Inverse-Hessian-Vector-Product Approximation Speed-Quality Trade-Off

Next, we look at the speed-quality trade-off of the Hessian approximation tricks. The goal is to see if

⁶Experiments in Sec. 6.2 find that when the predictions are incorrect, there tend to exist a few very-helpful data-points and many more relatively-medium harmful ones. This might help explain that k NN tends to have higher recall on helpful data-points when the predictions are incorrect.

the Hessian approximation’s speed-up comes at the cost of dramatically lower quality. Our experiments show that the speed-up does not greatly affect the quality.

Results. Figure 4 shows the results of the experiments. For the two figures on the left, we can observe that the computation cost (measured in time) grows with both the batch size and number of recursive iterations J . Similarly, the estimation error⁷ (the figure on the right) shows that the error decreases with both the batch size and J in general.

Further, we notice that when the batch size is small (e.g., $B=1$), we can make up the loss in quality by increasing T , which is inherently parallelizable (Sec. 3.4). Overall, these suggest that we could trade off a small drop in quality with a significant speed-up by the combination of (1) small B , (2) medium J , and (3) large T .⁸

5.3 Quality of Influence Estimations

Finally, we want to ensure that there are no significant cascading estimation errors and that the final

⁷The estimation error is measured as the difference norm w.r.t. the estimation using the most expensive configuration.

⁸We pick J in $\{1000, 2000\}$ based on convergence.

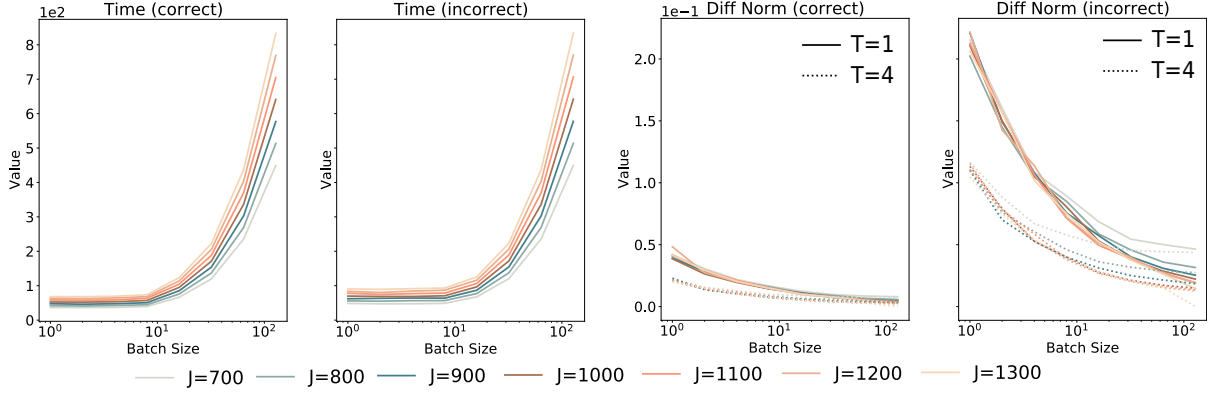


Figure 4: **Left Half:** computational time of Hessian approximation as a function of batch size and recursive iterations J . We further break down the figure into two sub-figures: cases when the prediction is correct and those when it is incorrect. **Right Half:** estimation error norm as a function of batch size, recursive iterations, whether the prediction is correct, and additionally the number of independent runs T .

Comparison	Pearson	Spearman	Kendall
Fast ($k = 10^3$) vs Full	99.9 ± 0.05	99.8 ± 0.39	97.4 ± 1.69
Fast ($k = 10^4$) vs Full	99.9 ± 0.04	99.9 ± 0.09	98.0 ± 0.77
Fast ($k = 10^3$) vs Fast ($k = 10^4$)	99.9 ± 0.08	99.8 ± 0.35	97.3 ± 1.66

Table 3: Correlations between influence values using various measures. The means and standard deviations are computed with 6 evaluation points (balanced between correct and incorrect predictions).

computed influence scores are of sufficient quality. Think of Sec. 5.1 and 5.2 as “unit-tests” to understand whether each component works well on its own, and in this section, our goal is to understand whether all the components work well together.

Specifically, we compute the correlations of influence values among the following two systems: one that computes influence functions with both k NN and fast s_{test} approximation (**Fast**, with $k=10^3/k=10^4$), and one that computes influence functions without them (**Full**). In the appendix, we further compare the quality of computed influences by actually retraining models.

Table 3 shows that the correlations are high for all measures considered. These demonstrate that using the fast influence functions achieve reasonable qualities at just a fraction of the total cost.

6 Experiments

In this section, we illustrate four applications of the fast influence functions: (1) examining the “explainability” of influential examples; (2) visualizing how different training data-points affect evaluation data-points; correcting model predictions via learning (3) on influential training examples, or (4) on influential data-points from a new dataset (data-augmentation).

6.1 Explainability of Influential Examples

Motivation. Despite being appealing for model interpretation, influence functions estimate the change in the test data-point loss function through up-weighting the loss of the training data-point. This is not a metric of model interpretation by itself, and thus naturally leads to the question: *to what extent can influential data-points be used to explain model predictions?*

Approach. While there are many notions of explainability, here we will mainly focus on the concept of *simulatability*. Doshi-Velez and Kim (2017) explained that a model is simulatable when a person can predict its behavior on new inputs. Here, we will measure an explanation’s quality in terms of its effect on model simulatability.

Unfortunately, conducting human studies to assess the simulatability is expensive in terms of time and cost, and hence not scalable. Here we use a simple approximation (Treviso and Martins, 2020; Hase et al., 2020): we learn another model (the simulator model) to *predict the predictions* of the model (the task model). The simulator model is trained with the same data as the task model, but the labels are replaced with the task model’s predictions. Then, we fine-tune the simulator on data identified as influential for the task model’s perfor-

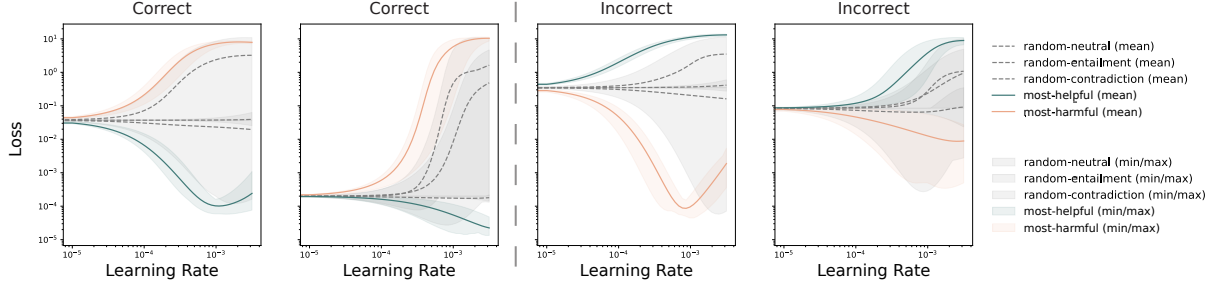


Figure 5: Simulator loss on 4 test data-points (more figures in the appendix), where the simulator is fine-tuned on different types of data-points with ground truth labels using various learning rates. The lines refer to the mean performance averaged across 10 fine-tuning data-points, and the shaded area covers the max/min performance.

mance on test data-points. If the simulator model can better predict what the task model will do by fine-tuning on this data (i.e., achieving lower loss), the influential data points are said to be a good “explanation” of the task model’s behavior. This approach is similar to Pruthi et al. (2020), who also treat explanations as targets to fit a model to.

Experiment Results. Figure 5 shows the final results.⁹ Here, the X-axis refers to the learning rate we use to fine-tune the simulator model, Y-axis refers to the simulator’s loss, and each line represents the type of data used in simulator fine-tuning. We can observe that when the prediction is correct, finetuning on helpful data-points significantly improves the simulator’s ability to predict the task model’s behavior. Similarly, when the prediction is incorrect, finetuning on data-points that are *harmful* (to the task model’s loss on ground-truth labels) *improves* the simulator’s predictions of the task model. Further, the effect on the loss from influential data-points is greater than the random selection of data-points overall. This demonstrates that influential examples can serve as explanations of the task model’s behavior.

6.2 Effect Visualization

Motivation. Investigating how different training data-points interact with test data-points is also useful, because such exploratory data analysis can discover interesting relationships between data-slices (i.e., subsets of data with specific attributes). For example, which subset of data is helpful to one particular subset of test data-points while being harmful to another, or what are the relationships between the subsets of data? To this end, a visualization of the interaction between training data-points

Slice	Average $ I $ ($\times 10^{-1}$)		# Edges ($\times 10^5$)	
	Helpful	Harmful	Helpful	Harmful
H (L)	8.66	0.34	0.05	0.95
H (S)	9.34	0.66	0.08	0.92
H (C)	4.65	1.79	0.29	0.71
M	136.89	44.19	0.27	0.73

Table 4: Statistics on the visualizations. Harmful edges have positive influences, helpful edges have negative influences, but here we use average absolute values (Average $|I|$). # Edges refers to the number of (harmful/helpful) edges connecting to the slice. “H (L/S/C)” refers to the lexical-overlap, subsequence, and constituent subset of HANS, and “M” to the 2-label version of MultiNLI. Note that for average $|I|$, comparisons are only meaningful within each row.

and test data-points will yield useful insights.

Approach. We conduct experiments on two models, one trained on MultiNLI and the other trained on the HANS dataset. We then compute influence functions on their corresponding training data-points and build circular bipartite graphs. The nodes represent training (outer circle) and evaluation (inner circles) data-points (incorrect predictions), and the strength and color of edges represent the influence values.

Experiment Results. Figure 6 visualizes the results, where the left half corresponds to the model trained on MultiNLI and the right half corresponds to the model trained on HANS.

Left Hand Side. Table 4 summarizes a few key statistics about the plots on the left hand side. Interestingly, we observe that while there are more MultiNLI training data-points that are harmful to HANS/MultiNLI evaluation data-points, their (harmful) influences are in general much lower than the helpful counterparts. This suggests that a few critical helpful data-points can potentially improve

⁹We visualize 4 test data-points here (2 correct, and 2 incorrect). Please see the appendix for the full visualizations.

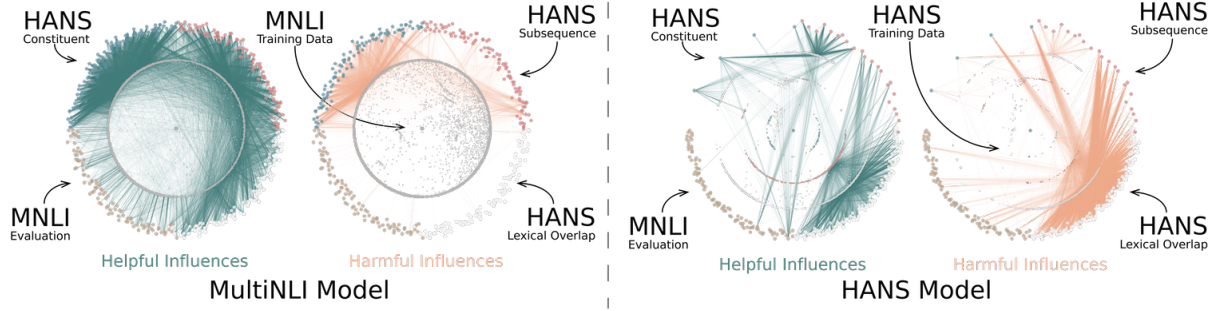


Figure 6: Visualization of the interaction between evaluation and training data-points. The graphs on the left half represent the model trained on MultiNLI, and the graphs on the right half represent the model trained on HANS. Within each half, the graphs on the left column represent connections with helpful influences, and the graphs on the right column represent connections with harmful connections. Note that the positions of outer/evaluation data points are fixed between two figures. However, the positions of inner/training data-points are not the same across the two figures. Instead, the positions are determined by minimizing the weighted distance (for visualization purposes).

Slice	HANS (L)	HANS (S)	HANS (C)	MNLI
Correlation (Rounded)				
H (L)	1.00	0.99	0.99	0.92
H (S)	0.99	1.00	0.99	0.91
H (C)	0.99	0.99	1.00	0.67
M	0.92	0.91	0.67	1.00
Number of Pairs				
H (L)	29581	14917	3425	5380
H (S)	14917	25145	6218	6270
H (C)	3425	6218	26621	13972
M	5380	6270	13972	72324

Table 5: Statistics on the correlations and number of pairs (where a training data-point have influences on both data slices) between data slices. “H (L/S/C)” refers to the lexical-overlap, subsequence, and constituent subset of HANS, and “M” to the 2-label version of MultiNLI.

the model’s performance on HANS. In contrast, a few harmful data-points will have a relatively lower impact on the model’s performance. In Sec. 6.3, we will leverage this insight to improve model performance on HANS. This could also be connected to the observation we have in Sec. 5.1 where the recall scores of k NN tend to be higher for helpful data-points for incorrect predictions.

Further, we measure the influence correlation between different data slices in Table 5.¹⁰ We can see from the table that the correlation is reasonably high between each pair of data slices, and in particular between HANS subsets. This suggests that, for the datasets considered here, if training data-points are influential (either harmful or helpful) to one of

¹⁰Please see the appendix regarding details on computing correlations.

the data slices, these data-points might be similarly influential to other data slices (if influential at all).

Right Hand Side. Since here the training data is HANS, we further segment the HANS training data-points based on the subset they are in, using different colors and radii. Interestingly, we can find that training data-points in the “Lexical Overlap” are noticeably more influential (either helpful and harmful) to all the HANS evaluation dataset subsets. Note that, by the construction of the dataset, the “Lexical Overlap” heuristic includes other heuristics as special cases. This conveys that effect visualization can be used to discover some latent structure in the dataset construction.

6.3 Error Correction

Motivation. In addition to model interpretation and exploratory data analysis, one might also consider ways to correct the wrong model predictions. This is often useful in practice, where practitioners both want to understand the problem and correct it. Luckily, the influence function not only implies which data-points are harmful (i.e., they have the potential to nudge the model to make the wrong prediction), but also which data-points that are helpful (i.e., they have the potential to nudge the model to make the right prediction). This suggests a simple way to correct/fix model predictions: taking gradient steps with the model on the helpful data-points. This method can be applied to correct/fix a single prediction or multiple predictions.

This approach naturally leads to another interesting question. Instead of taking gradient steps on data from the original data-points, can the same approach be used to suggest *new* training data-points

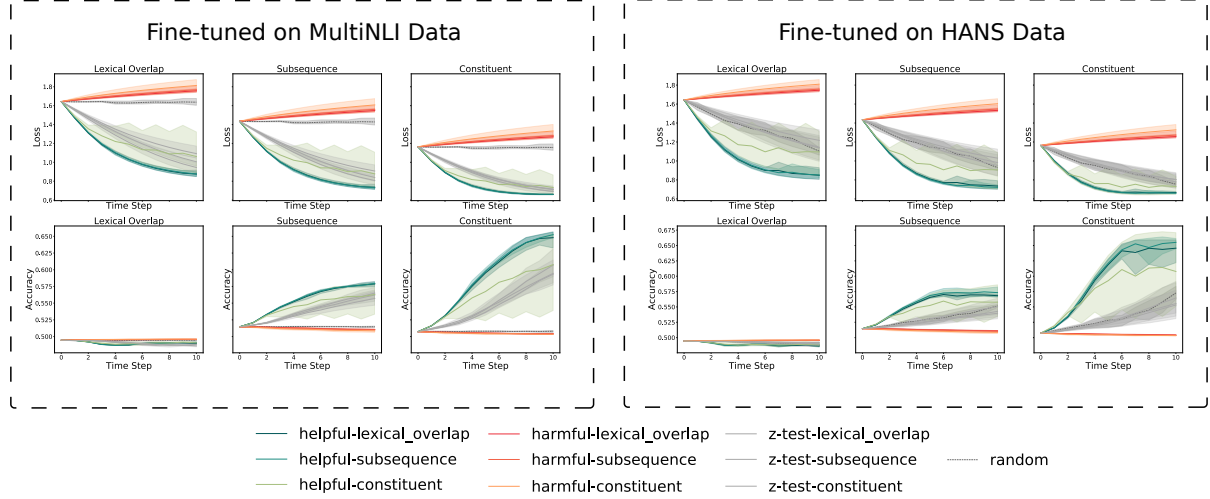


Figure 7: Performance on HANS dataset (lexical-overlap, subsequence, and constituent) after repeatedly taking gradient steps on different types of data-points from **MultiNLI** (left hand side) and **HANS** (right hand side) training set using influence functions, as well as on anchor data-points. The influence values are computed w.r.t. each subset of HANS evaluation dataset (shown with different line colors). The lines refer to the mean performance averaged across 3 repetition, and the shaded area covers the max/min performance.

that were not seen during training? This is interesting as the original formulations of influence functions are defined on the data-points used during training.¹¹ Here we examine the counterfactual scenarios: *how would the model performance change if we include the (new) data-points in the training dataset?* Our experiments show that, when the new training data-points are “similar” to the original training data-points, this approach can be helpful.

Approach. For a given dataset/data-slice and a small batch of evaluation data-points (“anchor” data-points), we (1) compute influence scores of training data-points w.r.t. the anchor data-points, and then (2) update model parameters by taking gradient steps on influential training data-points w.r.t. these anchor data-points. These two steps are repeatedly applied multiple times.

Experiment Results. Figure 7 shows the results for the model trained on MultiNLI and evaluated

on HANS.¹² The left figure refers to the setting where the augmented data come from the original training dataset (MultiNLI). We can see that fine-tuning on helpful data-points overall improves the performances compared to random ones, and fine-tuning on harmful data points leads to worse performances in general. Here, this simple technique brings more than 5% average improvement in accuracy.

Note that using influence functions requires gradient access to the anchor data-points; thus we also experiment with directly fine-tuning on them as well (“z-test” in the figure). The results demonstrate the potential of using influence functions to correct model predictions, above and beyond the improvements available from just finetuning on the anchor data-points (by about 2.6% in accuracy on average).

We can also observe from Figure 7 that helpful examples tend to have a greater magnitude of effect than harmful examples. This observation can be connected to the visualization results shown in Sec. 6.3 where we can see (a handful of) helpful data-points have large negative/helpful influences while many data-points have medium positive/harmful influences.

The right half in Fig. 7 shows the results for the

¹¹Recently, Yang et al. (2020) examined the application of influence functions in filtering out detrimental synthetic training examples. Here we focus on a related application of using them in selecting helpful training examples from another dataset (non-synthetic). Both of these experiments demonstrate that computing influence values on new examples could be useful. However, Yang et al. (2020) (Appendix C) reported that with a pool of more than 380K candidates, running influence functions could take more than 8 hours. In our experiment setup (i.e., finding a handful of influential examples), we can find the most helpful examples significantly faster thanks to our fast influence functions (see Sec. 3.5 for details). Extending our fast influence functions to their setup would be an interesting next-step.

¹²Note that while the losses on the lexical-overlap subset of HANS improve, the accuracies do not. This is because the predicted probabilities become more calibrated, but the output of the arg max operations do not. This still makes sense as the influence function is computed w.r.t. the loss.

same model evaluated on the same dataset. However, instead of fine-tuning the model on MultiNLI training data-points, here we fine-tune the model using HANS training data-points (i.e., the data augmentation setup). We can observe that, random data augmentation works reasonably well.¹³ Further, augmenting helpful HANS data-points can outperform random data augmentation and using anchor data-points directly in general – about 2.6% improvement on accuracy on average. These results show the potential of influence functions for sample-efficient data augmentation.¹⁴

7 Conclusions

In this work, we present FASTIF via simple modifications to influence functions that significantly speed up the computation without significantly impacting its performance. Our improvements include using k NN to pre-select a subset of influence-worthy data-points, identifying a set of hyperparameters for the inverse Hessian-vector-product estimation algorithm, and a parallel implementation that minimizes communication overhead. We empirically examine the effectiveness of these modifications. Then, with the availability of fast influence functions, we demonstrate a few interesting applications that were previously intractable. These include examining the “explainability” of influential data-points, visualizing data influence-interactions, correcting model predictions using original training data, and finally correcting model predictions using data from a new dataset.

Acknowledgments

We thank Shi Feng for helpful discussions. HG interned at Salesforce Research; PH and MB were supported by a Salesforce Research Faculty Grant, NSF-CAREER Award 1846185, and a Royster Society PhD Fellowship.

References

Naman Agarwal, Brian Bullins, and Elad Hazan. 2017. Second-order stochastic optimization for machine learning in linear time. *Journal of Machine Learning Research*, 18(116):1–40.

¹³This intuitively makes sense because the evaluation data comes from HANS evaluation dataset.

¹⁴Here we see little difference between augmenting with original training data (MultiNLI) or data from a new dataset (HANS), i.e., two approaches we discussed in this section. We leave investigating the possibility of better augmentation techniques to future works.

Samyadeep Basu, Philip Pope, and Soheil Feizi. 2020a. Influence functions in deep learning are fragile. *arXiv preprint arXiv:2006.14651*.

Samyadeep Basu, Xuchen You, and Soheil Feizi. 2020b. On second-order group influence functions for black-box predictions. In *International Conference on Machine Learning*, pages 715–724. PMLR.

Yonatan Belinkov and James Glass. 2019. Analysis methods in neural language processing: A survey. *Transactions of the Association for Computational Linguistics*, 7:49–72.

Marc-Étienne Brunet, Colleen Alkalay-Houlihan, Ashton Anderson, and Richard Zemel. 2019. Understanding the origins of bias in word embeddings. In *International Conference on Machine Learning*, pages 803–811. PMLR.

Oana-Maria Camburu, Tim Rocktäschel, Thomas Lukasiewicz, and Phil Blunsom. 2018. *e-snli: Natural language inference with natural language explanations*. In *NeurIPS 2018*.

Samprit Chatterjee, Ali S Hadi, et al. 1986. Influential observations, high leverage points, and outliers in linear regression. *Statistical science*, 1(3):379–393.

Chaofan Chen, Oscar Li, Daniel Tao, Alina Barnett, Cynthia Rudin, and Jonathan K Su. 2019. This looks like that: deep learning for interpretable image recognition. In *Advances in neural information processing systems*, pages 8930–8941.

Andreas Christmann and Ingo Steinwart. 2004. On robustness properties of convex risk minimization methods for pattern recognition. *Journal of Machine Learning Research*, 5(Aug):1007–1034.

R Dennis Cook. 1977. Detection of influential observation in linear regression. *Technometrics*, 19(1):15–18.

R Dennis Cook. 1986. Assessment of local influence. *Journal of the Royal Statistical Society: Series B (Methodological)*, 48(2):133–155.

R Dennis Cook and Sanford Weisberg. 1980. Characterizations of an empirical influence function for detecting influential cases in regression. *Technometrics*, 22(4):495–508.

R Dennis Cook and Sanford Weisberg. 1982. *Residuals and influence in regression*. New York: Chapman and Hall.

Michiel Debruyne, Mia Hubert, and Johan AK Suykens. 2008. Model selection in kernel based regression using the influence function. *Journal of Machine Learning Research*, 9(Oct):2377–2400.

Jacob Devlin, Ming-Wei Chang, Kenton Lee, and Kristina Toutanova. 2019. Bert: Pre-training of

- deep bidirectional transformers for language understanding. In *Proceedings of the 2019 Conference of the North American Chapter of the Association for Computational Linguistics: Human Language Technologies, Volume 1 (Long and Short Papers)*, pages 4171–4186.
- Finale Doshi-Velez and Been Kim. 2017. Towards a rigorous science of interpretable machine learning. *arXiv preprint arXiv:1702.08608*.
- Julian J Faraway. 2016. *Extending the linear model with R: generalized linear, mixed effects and non-parametric regression models*. CRC press.
- Vitaly Feldman and Chiyuan Zhang. 2020. What neural networks memorize and why: Discovering the long tail via influence estimation. *Advances in Neural Information Processing Systems*, 33.
- Shi Feng, Eric Wallace, Alvin Grissom II, Mohit Iyyer, Pedro Rodriguez, and Jordan Boyd-Graber. 2018. Pathologies of neural models make interpretations difficult. In *Proceedings of the 2018 Conference on Empirical Methods in Natural Language Processing*, pages 3719–3728.
- Amirata Ghorbani, Michael P Kim, and James Zou. 2020. A distributional framework for data valuation. *ICML*.
- Amirata Ghorbani and James Zou. 2019. Data shapley: Equitable valuation of data for machine learning. In *International Conference on Machine Learning*, pages 2242–2251.
- Xiaochuang Han, Byron C. Wallace, and Yulia Tsvetkov. 2020. [Explaining black box predictions and unveiling data artifacts through influence functions](#). In *ACL*.
- Peter Hase and Mohit Bansal. 2020. Evaluating explainable ai: Which algorithmic explanations help users predict model behavior? *ACL*.
- Peter Hase, Chaofan Chen, Oscar Li, and Cynthia Rudin. 2019. Interpretable image recognition with hierarchical prototypes. In *Proceedings of the AAAI Conference on Human Computation and Crowdsourcing*.
- Peter Hase, Shiyue Zhang, Harry Xie, and Mohit Bansal. 2020. Leakage-adjusted simulatability: Can models generate non-trivial explanations of their behavior in natural language? *Findings of EMNLP*.
- Trevor Hastie, Robert Tibshirani, and Jerome Friedman. 2009. *The elements of statistical learning: data mining, inference, and prediction*. Springer Science & Business Media.
- Sarthak Jain and Byron C Wallace. 2019. Attention is not explanation. In *Proceedings of the 2019 Conference of the North American Chapter of the Association for Computational Linguistics: Human Language Technologies, Volume 1 (Long and Short Papers)*, pages 3543–3556.
- Ruoxi Jia, David Dao, Boxin Wang, Frances Ann Hubis, Nezihe Merve Gürel, Bo Li, Ce Zhang, Costas Spanos, and Dawn Song. 2019a. Efficient task-specific data valuation for nearest neighbor algorithms. *Proceedings of the VLDB Endowment*, 12(11):1610–1623.
- Ruoxi Jia, David Dao, Boxin Wang, Frances Ann Hubis, Nick Hynes, Nezihe Merve Gürel, Bo Li, Ce Zhang, Dawn Song, and Costas J Spanos. 2019b. Towards efficient data valuation based on the shapley value. In *The 22nd International Conference on Artificial Intelligence and Statistics*, pages 1167–1176.
- Jeff Johnson, Matthijs Douze, and Hervé Jégou. 2017. Billion-scale similarity search with gpus. *arXiv preprint arXiv:1702.08734*.
- Shalmali Joshi, Oluwasanmi Koyejo, Been Kim, and Joydeep Ghosh. 2018. xgems: Generating examples to explain black-box models. *arXiv preprint arXiv:1806.08867*.
- Urvashi Khandelwal, Omer Levy, Dan Jurafsky, Luke Zettlemoyer, and Mike Lewis. 2019. Generalization through memorization: Nearest neighbor language models. In *International Conference on Learning Representations*.
- Been Kim, Martin Wattenberg, Justin Gilmer, Carrie Cai, James Wexler, Fernanda Viegas, et al. 2018. Interpretability beyond feature attribution: Quantitative testing with concept activation vectors (tcav). In *International conference on machine learning*, pages 2668–2677. PMLR.
- Sosuke Kobayashi, Sho Yokoi, Jun Suzuki, and Kentaro Inui. 2020. [Efficient estimation of influence of a training instance](#). In *Proceedings of SustaiNLP: Workshop on Simple and Efficient Natural Language Processing*, pages 41–47, Online. Association for Computational Linguistics.
- Pang Wei Koh and Percy Liang. 2017. Understanding black-box predictions via influence functions. In *Proceedings of the 34th International Conference on Machine Learning-Volume 70*, pages 1885–1894. JMLR. org.
- Pang Wei Koh, Jacob Steinhardt, and Percy Liang. 2018. Stronger data poisoning attacks break data sanitization defenses. *arXiv preprint arXiv:1811.00741*.
- Pang Wei W Koh, Kai-Siang Ang, Hubert Teo, and Percy S Liang. 2019. On the accuracy of influence functions for measuring group effects. In *Advances in Neural Information Processing Systems*, pages 5254–5264.
- Yongchan Kwon, Manuel A Rivas, and James Zou. 2020. Efficient computation and analysis of distributional shapley values. *arXiv preprint arXiv:2007.01357*.

- Jaeeun Lee, Raphael Tang, and Jimmy Lin. 2019. What would elsa do? freezing layers during transformer fine-tuning. *arXiv preprint arXiv:1911.03090*.
- Jiwei Li, Xinlei Chen, Eduard Hovy, and Dan Jurafsky. 2016a. [Visualizing and Understanding Neural Models in NLP](#). In *Proceedings of the 2016 Conference of the North American Chapter of the Association for Computational Linguistics: Human Language Technologies*, pages 681–691. Association for Computational Linguistics.
- Jiwei Li, Will Monroe, and Dan Jurafsky. 2016b. Understanding neural networks through representation erasure. *arXiv preprint arXiv:1612.08220*.
- Zachary C. Lipton. 2016. [The mythos of model interpretability](#). In *2016 ICML Workshop on Human Interpretability in Machine Learning*.
- Yong Liu, Shali Jiang, and Shizhong Liao. 2014. Efficient approximation of cross-validation for kernel methods using bouligand influence function. In *International Conference on Machine Learning*, pages 324–332.
- Scott M Lundberg and Su-In Lee. 2017. [A Unified Approach to Interpreting Model Predictions](#). In *Advances in Neural Information Processing Systems 30*, pages 4765–4774.
- Tom McCoy, Ellie Pavlick, and Tal Linzen. 2019. Right for the wrong reasons: Diagnosing syntactic heuristics in natural language inference. In *Proceedings of the 57th Annual Meeting of the Association for Computational Linguistics*, pages 3428–3448.
- Yuxian Meng, C. Fan, Zijun Sun, E. Hovy, Fei Wu, and J. Li. 2020. [Pair the dots: Jointly examining training history and test stimuli for model interpretability](#). *ArXiv*, abs/2010.06943.
- Ramaravind K Mothilal, Amit Sharma, and Chenhao Tan. 2020. Explaining machine learning classifiers through diverse counterfactual explanations. In *Proceedings of the 2020 Conference on Fairness, Accountability, and Transparency*, pages 607–617.
- Chris Olah, Nick Cammarata, Ludwig Schubert, Gabriel Goh, Michael Petrov, and Shan Carter. 2020. [An overview of early vision in inceptionv1](#). *Distill*. <https://distill.pub/2020/circuits/early-vision>.
- Chris Olah, Arvind Satyanarayan, Ian Johnson, Shan Carter, Ludwig Schubert, Katherine Ye, and Alexander Mordvintsev. 2018. [The Building Blocks of Interpretability](#). *Distill*, 3(3):e10.
- Nicolas Papernot and Patrick McDaniel. 2018. [Deep k-Nearest Neighbors: Towards Confident, Interpretable and Robust Deep Learning](#). *arXiv:1803.04765 [cs, stat]*. *ArXiv*: 1803.04765.
- Adam Paszke, Sam Gross, Francisco Massa, Adam Lerer, James Bradbury, Gregory Chanan, Trevor Killeen, Zeming Lin, Natalia Gimelshein, Luca Antiga, Alban Desmaison, Andreas Kopf, Edward Yang, Zachary DeVito, Martin Raison, Alykhan Tejani, Sasank Chilamkurthy, Benoit Steiner, Lu Fang, Junjie Bai, and Soumith Chintala. 2019. [Pytorch: An imperative style, high-performance deep learning library](#). In *Advances in Neural Information Processing Systems 32*, pages 8024–8035. Curran Associates, Inc.
- Danish Pruthi, Bhuwan Dhingra, Livio Baldini Soares, Michael Collins, Zachary C. Lipton, Graham Neubig, and William W. Cohen. 2020. [Evaluating explanations: How much do explanations from the teacher aid students?](#) *CoRR*, abs/2012.00893.
- Nazneen Fatema Rajani, Ben Krause, Wengpeng Yin, Tong Niu, Richard Socher, and Caiming Xiong. 2020. Explaining and improving model behavior with k nearest neighbor representations. *arXiv preprint arXiv:2010.09030*.
- Nazneen Fatema Rajani, Bryan McCann, Caiming Xiong, and Richard Socher. 2019. [Explain yourself! leveraging language models for commonsense reasoning](#). In *ACL 2019*.
- Marco Tulio Ribeiro, Sameer Singh, and Carlos Guestrin. 2016a. "why should i trust you?" explaining the predictions of any classifier. In *Proceedings of the 22nd ACM SIGKDD international conference on knowledge discovery and data mining*, pages 1135–1144.
- Marco Tulio Ribeiro, Sameer Singh, and Carlos Guestrin. 2016b. ["Why Should I Trust You?": Explaining the Predictions of Any Classifier](#). *Knowledge Discovery and Data Mining (KDD)*.
- Marco Tulio Ribeiro, Sameer Singh, and Carlos Guestrin. 2018a. [Anchors: High-precision model-agnostic explanations](#). In *AAAI Conference on Artificial Intelligence*.
- Marco Tulio Ribeiro, Sameer Singh, and Carlos Guestrin. 2018b. Anchors: High-precision model-agnostic explanations. In *AAAI*.
- Marco Tulio Ribeiro, Tongshuang Wu, Carlos Guestrin, and Sameer Singh. 2020. Beyond accuracy: Behavioral testing of nlp models with checklist. In *Association for Computational Linguistics (ACL)*.
- Pouya Samangouei, Ardavan Saeedi, Liam Nakagawa, and Nathan Silberman. 2018. Explaingan: Model explanation via decision boundary crossing transformations. In *Proceedings of the European Conference on Computer Vision (ECCV)*, pages 666–681.
- Peter Schulam and Suchi Saria. 2019. Can you trust this prediction? auditing pointwise reliability after learning. In *The 22nd International Conference on Artificial Intelligence and Statistics*, pages 1022–1031.

- Avanti Shrikumar, Peyton Greenside, and Anshul Kundaje. 2017. Learning important features through propagating activation differences. In *International Conference on Machine Learning*, pages 3145–3153.
- Karen Simonyan, Andrea Vedaldi, and Andrew Zisserman. 2013. Deep inside convolutional networks: Visualising image classification models and saliency maps. *Workshop at International Conference on Learning Representations*.
- Karen Simonyan, Andrea Vedaldi, and Andrew Zisserman. 2014. [Deep inside convolutional networks: Visualising image classification models and saliency maps](#). In *Workshop at International Conference on Learning Representations*.
- Daniel Smilkov, Nikhil Thorat, Been Kim, Fernanda Viégas, and Martin Wattenberg. 2017. Smoothgrad: removing noise by adding noise. *arXiv preprint arXiv:1706.03825*.
- Mukund Sundararajan, Ankur Taly, and Qiqi Yan. 2017a. [Axiomatic Attribution for Deep Networks](#). In *Proceedings of the 34th International Conference on Machine Learning - Volume 70*.
- Mukund Sundararajan, Ankur Taly, and Qiqi Yan. 2017b. Axiomatic attribution for deep networks. In *International Conference on Machine Learning*, pages 3319–3328.
- William Thomas and R Dennis Cook. 1990. Assessing influence on predictions from generalized linear models. *Technometrics*, 32(1):59–65.
- Marcos Treviso and André F. T. Martins. 2020. [The explanation game: Towards prediction explainability through sparse communication](#). In *Proceedings of the Third BlackboxNLP Workshop on Analyzing and Interpreting Neural Networks for NLP*, pages 107–118, Online. Association for Computational Linguistics.
- Eric Wallace, Jens Tuyls, Junlin Wang, Sanjay Subramanian, Matt Gardner, and Sameer Singh. 2019. Allennlp interpret: A framework for explaining predictions of nlp models. In *Proceedings of the 2019 Conference on Empirical Methods in Natural Language Processing and the 9th International Joint Conference on Natural Language Processing (EMNLP-IJCNLP): System Demonstrations*, pages 7–12.
- Bo-Cheng Wei, Yue-Qing Hu, and Wing-Kam Fung. 1998. Generalized leverage and its applications. *Scandinavian Journal of statistics*, 25(1):25–37.
- Sarah Wiegreffe, Ana Marasovic, and Noah A. Smith. 2020. [Measuring association between labels and free-text rationales](#). *CoRR*, abs/2010.12762.
- Sarah Wiegreffe and Yuval Pinter. 2019. Attention is not not explanation. In *Proceedings of the 2019 Conference on Empirical Methods in Natural Language Processing and the 9th International Joint Conference on Natural Language Processing (EMNLP-IJCNLP)*, pages 11–20.
- Adina Williams, Nikita Nangia, and Samuel R Bowman. 2018. A broad-coverage challenge corpus for sentence understanding through inference. In *Proceedings of NAACL-HLT*, pages 1112–1122.
- Thomas Wolf, Lysandre Debut, Victor Sanh, Julien Chaumond, Clement Delangue, Anthony Moi, Pierric Cistac, Tim Rault, Rémi Louf, Morgan Funtowicz, et al. 2019. Huggingface’s transformers: State-of-the-art natural language processing. *ArXiv*, pages arXiv–1910.
- Yiben Yang, Chaitanya Malaviya, Jared Fernandez, Swabha Swayamdipta, Ronan Le Bras, Ji-Ping Wang, Chandra Bhagavatula, Yejin Choi, and Doug Downey. 2020. G-daug: Generative data augmentation for commonsense reasoning. In *Findings of EMNLP*.
- Ruiqi Zhong, Steven Shao, and Kathleen McKeown. 2019. Fine-grained sentiment analysis with faithful attention. *arXiv preprint arXiv:1908.06870*.

Appendix

A Analysis

A.1 Recall of k NN

Details. For each evaluation data-point z_{test} , we first compute the ground-truth influential data-points via running influence functions on the MultiNLI training dataset without k NN (i.e., $\{\text{top-}m \text{ influential}\}$). Then, we use k NN to select the k training data-points (i.e., $\{\text{retrieved}\}$). We chose $k \in \{1 \times 10^1, 1 \times 10^2, 1 \times 10^3, 1 \times 10^4, 5 \times 10^4, 1 \times 10^5\}$. Finally, we compute the recall $R@m$ with $m \in \{10^1, 10^2, 10^3\}$. We repeat the aforementioned steps for three types of influential data-points: most positively influential (harmful), most negatively influential (helpful), and most influential (unsigned influence, by taking the absolute value). We select 100 data-points from the MNLI evaluation dataset (50 data-points when the model predictions are correct, 50 when they are incorrect) and aggregate the results.

A.2 Inverse-Hessian-Vector-Product Approximation Speed-Quality Trade-Off

Details. We compute the Hessian approximations with various configurations: $J \in \{700, 800, \dots, 1300\}$, $B \in \{2^0, 2^1, \dots, 2^7\}$, $T \in \{1, 2, 3, 4\}$ ¹⁵, and repeat the experiments for 8 different MultiNLI evaluation data-points (4 when the prediction is correct, and 4 when it is incorrect).

A.3 Quality of Influence Estimations

Here, we further compare the quality of computed influences by actually retraining the models using three systems: (1) a system that computes influence functions with both k NN and fast s_{test} approximation, (2) a system that computes influence functions without them, and (3) a system that randomly selects data-points.

Specifically, for each evaluation data-point selected, we find its m_{remove} most influential training data-points. Then we retrain the model by removing them and measure the change in the loss on the same evaluation data-point. If the influence function correctly identifies helpful and harm-

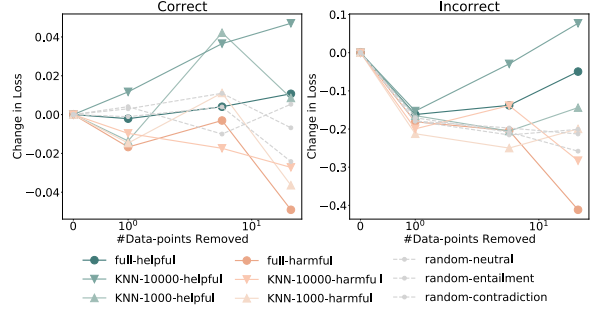


Figure 8: Change in loss on the data-point after re-training, where we remove $m_{\text{remove}} \in \{5^0, 5^1, 5^2\}$ data-points. We can see that the fast influence algorithms produce reasonable quality estimations at just a fraction of computation cost.

ful data-points, retraining without helpful points should result in the evaluation loss rising (i.e., positive change in loss), and retraining without harmful points should result in the loss falling (i.e., negative change in loss).

Details. For each evaluation data-point selected, we find its influential training data-points using one of the three aforementioned systems. Then we retrain the model by removing m_{remove} training data-point(s) and measure the change in the loss on the same evaluation data-point. For system (1), we use k NN (with $k=10^3, k=10^4$) and fast s_{test} approximation, and for system (3), we randomly select data-points with each of the three labels. We choose $m_{\text{remove}} = \{5^0, 5^1, 5^2\}$ and repeat the experiment for 6 data-points (3 for data-points where the prediction is correct, and 3 where it is incorrect).¹⁶

Results. Figure 8 shows the results, where we separate the results for cases based on whether the prediction is correct, and averaged across data-points within this bucket.¹⁷ We can see that overall loss increases when we remove helpful data, decreases when we remove harmful data-points. Further, the performance (measured by the change in loss) between using the fast influence functions and full influence functions (i.e., no k NN and fast s_{test} approximation) is similar, and both perform better than random selection in general.

¹⁵In the figures, we only include the results of different T for difference norm. This is because practitioners can use parallelism to speed up the computations of each run, which is independent of each other as described in Sec. 3.4. Thus, the change in time mainly depends on parallelism overhead, which we found to be reasonable in our initial experiments.

¹⁶These are the same 6 evaluation data-points used for computing correlations in the main paper.

¹⁷In the figure corresponding to incorrect predictions, we can see a decrease in the loss when we remove 1 data-point regardless of what type it is. We found that this is mostly influenced by the results on one of the evaluation data-points.

B Experimental Details

B.1 Explainability of Influential Examples

Experiment Design. To make the protocol more concrete, the evaluation method can be procedurally described as the following.

1. Train a model $f_{\theta_{\text{task}}}$ on the original training dataset $\{x_i, y_i\}_{i=1}^n$, and denote this model as the “task model”.
2. Train another model $f_{\theta_{\text{simulator}}}$ on the modified training dataset $\{x_i, \hat{y}_i\}_{i=1}^n$, where $\hat{y}_i = f_{\theta_{\text{task}}}(x_i)$ is the task model’s prediction. Denote this model as the “simulator model.”
3. Given a new test data-point x' and the task model’s prediction, compute the simulator model loss $\ell = L\left(f_{\theta_{\text{simulator}}}(x'), f_{\theta_{\text{task}}}(x')\right)$.
4. Find the most influential data-point(s), and further fine-tune (i.e., take gradient steps with) the simulator model on these data-point(s), to get new parameters $\theta'_{\text{simulator}}$. Compute the new simulator model loss $\ell' = L\left(f_{\theta'_{\text{simulator}}}(x'), f_{\theta_{\text{task}}}(x')\right)$.
5. Use the difference between ℓ and ℓ' as the proxy measure of explainability. The intuition is that the difference estimates how much extra information the explanation provides to the simulator model to forecast the task model’s prediction.

Details We repeat the experiments over 20 test data-points (10 when the prediction is correct, 10 when the prediction is incorrect), and choose five types of data for fine-tuning: random (with label neutral, entailment, or contradiction), most negative influential, and most positive influential. For a given test data-point and fine-tuning type, we fine-tune on 1 data-point with 50 learning rates in log-space from 10^{-5} to $10^{-2.5}$, and repeat for 10 different fine-tuning data-points. The max and mins losses among the 10 fine-tuning data-points are used to construct the confidence intervals. Further, during the fine-tuning, the label we used corresponds to the true label (instead of the label predicted by the model).¹⁸

¹⁸We experimented with both settings, and found using the original/true labels performed better. This makes sense as the task model was trained with true label as targets, and fitting to the original labels replicates the process that produced the task model.

Extended Results Please see Fig. 9 for extended visualizations.

B.2 Effect Visualization

Experiment Design. We conduct experiments on two models, one trained on MultiNLI and the other trained on the HANS dataset. We then compute influence functions on their corresponding training data-points and build circular bipartite graphs. The nodes represent training (outer circle) and evaluation (inner circles) data-points, and edges represent the influence values. For visualization purposes, we organize the nodes so that positions of training data-points are determined via optimizing a weighted distance function to their connected test data-points. In the setting with the model trained on HANS, we further partition the training data-points (represented by three inner circles) based on the subset they are in. Note that, this is possible only because the influence function calculations are fast enough.

Details. In both settings (i.e., visualizations corresponding to the model trained on MultiNLI and HANS dataset), we select 400 test data-points where the model predictions are incorrect, including 100 from the MNLI evaluation dataset and 100 for each of the three subsets from the HANS evaluation dataset. We use k NN with $k = 10^3$.

Details on Computing Correlations. We slightly abuse the notation and define $\bar{\mathcal{L}}_{i,j}$ as the average (signed) influence values between the i^{th} training data-point and j^{th} data slice. Note that each training data-point can influence multiple evaluation data-points. We then compute the correlation between each of the two pairs of data slices $\rho(\bar{\mathcal{L}}_{\cdot,j_1}, \bar{\mathcal{L}}_{\cdot,j_2})$. We only include cases where the data-point has influences on both data slices.

B.3 Error Correction

Experiment Design. The method can be described as follows:

1. For a given dataset (or a slice of it), first evaluate the model performance on the data slice.
2. Next, select a small batch of data-points from the evaluation dataset/data-slice as the “anchor” data-points.
3. Then, find influential data-point(s) from the training dataset w.r.t. those anchor data-points using influence functions.

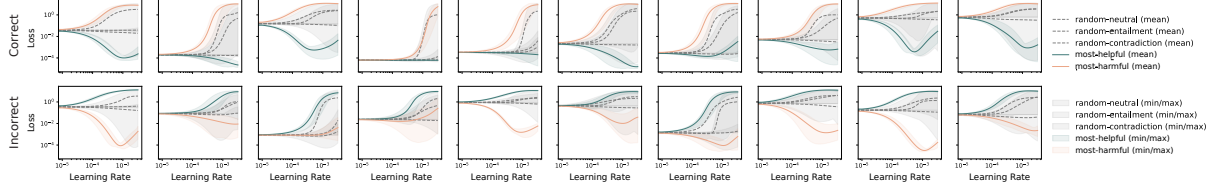


Figure 9: Simulator loss on 20 test data-points, where the simulator is fine-tuned on different types of data-points with ground truth labels using various learning rates. The solid line refer to the mean performance averaged across 10 fine-tuning data-points, and the dashed area covers the max/min performance.

4. Update the model parameters by taking gradient step(s) on these influential data-point(s).
5. Repeat Step 3-4 multiple times.
6. Re-evaluate the model performance on the data-slice (instead of the batch selected earlier for computing influence scores).

(original training data) or HANS (data augmentation), and we sample a batch size of 10 from evaluation data (i.e., the “anchor” data-points) when computing influence scores. We repeat the Step 3-4 for 10 iterations, and for each iteration, update parameters for one gradient step on 10 data-point with learning rate 10^{-4} .

Why Fine-tuning? In the ideal scenario, one intuitive way to correct model predictions given influential examples is to retrain the model with these examples added to the training dataset. However, this is expensive as one could imagine.

To see why fine-tuning on influential examples makes sense, recall the definition of influence functions on model parameters (Koh and Liang, 2017),

$$\mathcal{I}_{\text{params}}(z) := \left. \frac{d\hat{\theta}_{\epsilon,z}}{d\epsilon} \right|_{\epsilon=0} \approx -H_{\hat{\theta}}^{-1} \nabla_{\theta} L(z, \hat{\theta}) \quad (10)$$

We can see that by setting the (matrix) learning rate proportional to $-H_{\hat{\theta}}^{-1}$, fine-tuning on influential examples is an approximation of retraining the model with the loss of influential examples upweighted. In practice, computing the Hessian inverse for each gradient update is expensive, so we could use a scalar learning rate instead (e.g., through diagonal approximation). This reduces to the vanilla fine-tuning setting.

Details. The experiment is repeated 3 times, and compare the performance between using helpful data-points, harmful data-points, and random data-points. Since we assume gradient access to the anchor data-points, we further experiment with directly fine-tuning on those anchor data-points.

In our experiments, we use each of the three slices of the HANS dataset as the evaluation dataset and the model trained on MultiNLI as the base model. The training data used in influence-functions-based fine-tuning is either MultiNLI